

Self-Repair and Patterning of 2D Membrane-Like Peptoid Materials

Fang Jiao, Yulin Chen, Haibao Jin, Pingang He, Chun-Long Chen,*
and James J. De Yoreo*

Due to their unique physical and chemical properties, 2D materials have attracted intense interest for applications in filtration, sensing, nanoelectronics, and biomedical devices. Peptoids are a class of biomimetic sequence-defined polymers for which certain amphiphilic sequences self-assemble into 2D crystalline materials with properties that mimic those of cell membranes. In this study the ability of these membrane-like materials to self-repair following damage on a range of substrates is explored. In situ atomic force microscopy (AFM) is used to both create damage and image the subsequent repair process. Damage is induced by using the AFM to scribe peptoid-free patterns within a preassembled membrane. The results show here that, upon introduction of a peptoid-containing solution, for a suitable range of pH conditions, the damage is eliminated through assembly of the peptoids at the newly created edges, regardless of whether the substrates are negatively or positively charged and even in the absence of an underlying surface. The rate of the advancing edge depends on the edge orientation, the pH, and the composition of the substrate. Moreover, if the solution contains a second peptoid having an identical sequence in the hydrophobic block, repair of the defects results in nanoscale patterns of the new peptoid, even if the hydrophilic regions are distinct. Consequently, this ability to self-repair can be exploited to create nm-sized patterns of distinct functional groups within a single coherent membrane.

Polymer-based 2D materials are especially promising as templates for bottom-up assembly of nanostructured semiconductors, electronic circuits, organic–inorganic composites,^[5–7] and high surface area membranes for applications in filtration, chemical sensing, and catalysis.^[8,9] Taking inspiration from nature, many materials' characteristics, such as pores, metal or protein recognition sites, and other reactive groups^[4,10,11] have been introduced directly into polymer sequences to achieve molecular-scale control over their positions and dimensions. However, using these biomimetic 2D materials to truly emulate living systems requires the ability to create multifunctional membranes that exhibit multiple molecular-scale building blocks distributed on the nanoscale, as well as the capacity for self-repair. Though self-repair has been demonstrated for peptide-based materials assembled on mica,^[12] only quasi-1D nanofilaments of uniform composition were formed. Here we investigate both self-repair and the creation of multifunctional membranes in peptoid-based 2D materials.

Polypeptides are a class of biomimetic sequence specific polymers based on an N-substituted glycine backbone.^[13,14] The structure of a peptoid monomer is close to that of natural amino acids except that the side chains are appended to the amide nitrogen rather than the alpha carbon. Compared with polypeptides, peptoids lack both chirality and hydrogen-bond donors in the backbone. This difference results in a flexible chain with control over desired interactions through introduction of specific side chains. It also confers peptoids with excellent thermal and chemical stability.^[15] Synthesized via a solid-phase submonomer synthesis method from a chemically diverse set of cheap, commercially available building blocks,^[13,16] peptoids have an exact monomer sequence that can direct chain folding into higher order nanostructures.^[17,18] Peptoids were recently shown to assemble into so-called “nanosheets”.^[19–22] However, designs explored to date have not exhibited either the ability to self-repair or coassemble with other peptoids to form multifunctional materials.

We recently succeeded in synthesizing a new class of 2D materials from three peptoids (Pep-2, Pep-3, and Pep-4)

1. Introduction

Organic 2D materials are emerging biocompatible materials that can be chemically tailored through the self-assembly of small molecules, protein, or polymer building blocks.^[1–4]

F. Jiao, Prof. P. He
School of Chemistry and Molecular Engineering
East China Normal University
Shanghai 200241, China

F. Jiao, Dr. Y. Chen, Dr. H. Jin, Dr. C.-L. Chen,
Dr. J. J. De Yoreo
Physical Sciences Division
Pacific Northwest National Laboratory
Richland, WA 99352, USA
E-mail: chunlong.chen@pnl.gov; james.deyoreo@pnl.gov
Dr. J. J. De. Yoreo
Department of Materials Science and Engineering
University of Washington
Seattle, WA 98195, USA



DOI: 10.1002/adfm.201602365

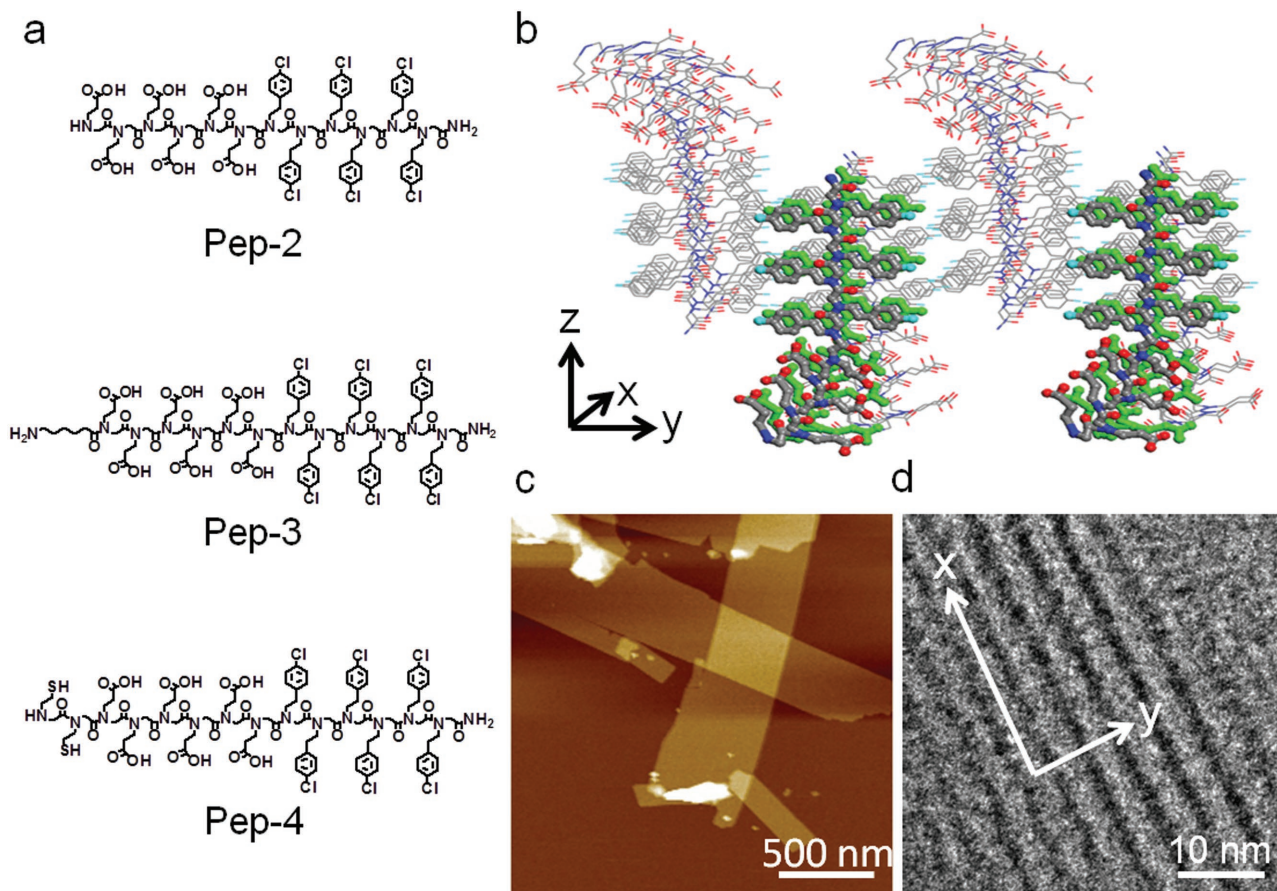


Figure 1. Self-assembly of diblock-like peptoids into 2D membranes. a) Structures of Pep-2–Pep-4. b) Molecular model showing proposed packing of Pep-2 inside membranes. c) AFM image of self-assembled Pep-3 membranes. d) A high-resolution TEM image showing well-aligned strips in the Pep-4 membrane structure.

(Figure 1a) that have an amphiphilic structure akin to the lipids that form bilayer cell membranes.^[23] (For detailed information on the synthesis and analysis of these peptoids, including HPLC (high performance liquid chromatography) and ESI-MS data, see the Supporting Information of ref. [23]) Membranes assembled from Pep-2 to Pep-4 exhibited sizes ranging from hundreds of nanometers to several micrometers in length and width. Under dry conditions, the thicknesses of these membranes is in the range of 3.5–4.0 nm, but can be increased to 4.2–5.4 nm through the introduction of NaCl or phosphate buffer solution (PBS). Based on both X-ray diffraction (XRD) data and molecular dynamics simulations^[23–27] the structure of these membranes was proposed to consist of alternating rows, half of which are oriented up along the z-axis and half oriented down, with extensive π -stacking in the hydrophobic *N*-[2-(4-chlorophenyl)ethyl]glycines ($N_{4-Cl}pe$) region and disorder in the carboxy tails (Figure 1b). The packing within each row was found to be anisotropic with the sidechains oriented along the y-axis, and the phenyl groups stacked along the x-axis. transmission electron microscopy (TEM) data (Figure 1d) supports this model, showing that Pep-4 forms well-aligned strips along the x-direction. AFM studies show these biomimetic membranes possess very straight edges along the x-direction and a rougher edge along the y-direction

and are longer along x than y (Figure 1c); this aspect ratio shows peptoid assembly into the membranes is faster along the x-direction than the y-direction. The observation of many over-lapping membranes when deposited on a substrate indicates they are free-standing in solution (Figure 1c). These membranes exhibit high stability when exposed to a range of solvents including ethanol, acetonitrile, and high ionic strength buffers, as well as high temperature (60 °C) and can self-repair when damaged.^[23]

To investigate the ability and mechanism of self-repair by these membrane-like materials for a range of substrates and solution conditions, we deposited preformed, free-standing membranes on substrates comprised of either atomically flat mica, which is hydrophilic, or highly ordered pyrolytic graphite (HOPG), which is hydrophobic. In the case of mica, we also investigated the effect of functionalizing the bare, negatively charged surface with (3-aminopropyl)triethoxysilane (APS) to produce a positively charged hydrophilic surface.

The membranes were scribed with an AFM in water to create a series of peptoid-free linear gaps running both along and across the peptoid rows, as well as at 45° (Figure 2). These gaps were tens of nm in width and their lengths varied from several nanometers to micrometers depending on the size of the as-deposited free-standing membrane. We found that

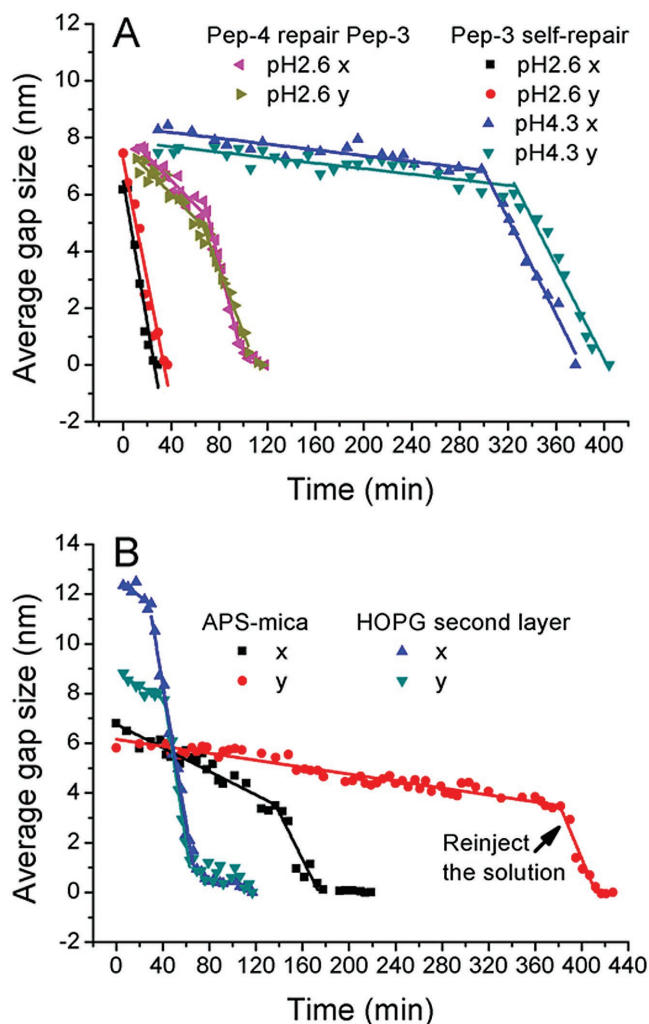


Figure 4. Peptoid repair rates depend on both the pH and the substrate upon which repair takes place. a) Effect of pH and type of peptoid used for repair. b) Effect of substrate composition.

repair along the x -direction being faster than along the y -direction (Figure 4 and Figure S M1, Supporting Information).

In order to determine the impact of the protonation state of the peptoid head groups on repair, we investigated the effect of pH over a pH range for which the mica surface remains strongly negative.^[28] When the pH was increased to 4.3, Pep-3 repair rates dropped dramatically (Figure 4a and Figure S M1, Supporting Information). Moreover, two distinct phases of repair were observed along both the x - and y -directions (Figure 4a, Table 1), with repair during the first stage being an order of magnitude slower than during the second stage. As was the case at pH 2.6, repair along the x -direction was slightly faster than along the y -direction during both stages. In addition, the transition to the second stage occurred earlier along the x -direction. Upon increasing the peptoid monomer concentration from 10×10^{-6} to 15×10^{-6} M at this same pH, the rates in both directions increased and repair once again occurred in a single stage (Table 1).

We also investigated the extent to which surface charge and hydrophobicity impacts the ability of the peptoids to adsorb and attach to the membrane edges. To investigate the impact of surface charge, we functionalized the mica surface, which normally possesses a large negative surface charge, with APS to give it a positive surface charge. The results for 10×10^{-6} M pH 4.3 Pep-3 monomer solution show that repair still proceeds (Figure 5a–f) and does so at a higher rate in both directions and in both stages of repair (Figure 4b, Table 1). However, while repair rates generally increased by only a small factor ($1.02 \times$ to $1.5 \times$), the rate of repair during first stage along the x -direction increased by over 400%. In contrast, the rate of repair during first stage along the y -direction remained slow and no transition to the second stage was observed until new solution was introduced into the cell after 400 min. These results demonstrate that peptoid membranes can self-repair on both positively and negatively charged hydrophilic surfaces, but that repair rates are anisotropic and, in either direction and during either stage of repair, can be altered by changing the peptoid concentration or the solution pH.

Table 1. Repair rates for Pep-3 membranes on various surfaces repaired by either Pep-2, Pep-3, or Pep-4.

Surface	Name	Grow velocity [nm min ⁻¹]			
		x -direction		y -direction	
		Stage 1	Stage 2	Stage 1	Stage 2
Mica	Pep-3 repair in 10×10^{-6} M Pep-3 pH 2.6	0.28 ± 0.03		0.23 ± 0.02	
	Pep-3 repair in 10×10^{-6} M Pep-3 pH 4.3	0.0051 ± 0.0006	0.084 ± 0.004	0.0046 ± 0.0006	0.076 ± 0.006
	Pep-3 repair in 15×10^{-6} M Pep-3 pH 4.3	0.19 ± 0.01		0.11 ± 0.01	
	Pep-3 repair in 10×10^{-6} M Pep-2 pH 4.3	≥0.90		≥0.72	
	Pep-3 repair in 20×10^{-6} M Pep-4 pH 2.6	0.044 ± 0.04	0.17 ± 0.01	0.044 ± 0.04	0.12 ± 0.01
	Pep-3 repair in 20×10^{-6} M Pep-4 pH 4.3	<0.01		<0.01	
APS-mica	Pep-3 repair in 10×10^{-6} M Pep-3 pH 4.3	0.021 ± 0.002	0.088 ± 0.014	0.0071 ± 0.0003	0.094 ± 0.01
Without underlying surface	Pep-3 repair in 40×10^{-6} M Pep-3 pH 2.6	0.038 ± 0.011	0.28 ± 0.01	0.025 ± 0.004	0.28 ± 0.02
	Pep-3 repair in 20×10^{-6} M Pep-3 pH 2.6	<0.022		<0.003	

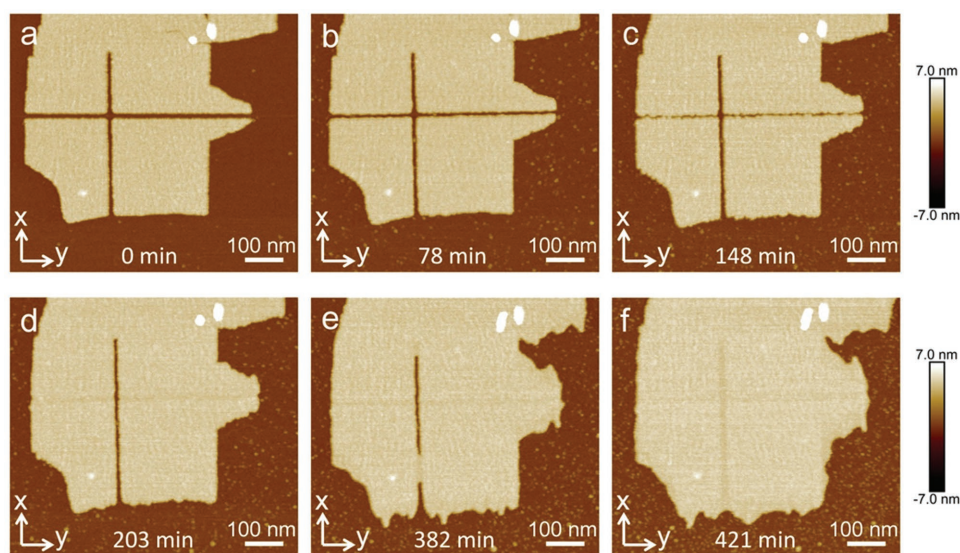


Figure 5. Peptoid membranes self-repair on APS-mica surfaces. a–f) In situ AFM images at different time points showing the anisotropic self-repair of Pep-3 membranes with mechanically introduced defects along x -, y -directions, in which the repair rate along x -direction was bigger than along the other direction.

To examine whether these 2D materials can self-repair on hydrophobic surfaces, we attempted to repair Pep-3 membranes on HOPG surfaces (Figure 6 and Figure S1, Supporting Information). When single layers of Pep-3 membranes placed on HOPG were damaged and the exposed to 10×10^{-6} M pH 4.3 Pep-3 monomer solution, no repair was observed for over 12 h (data not shown). Even when the pH was decreased to 2.6 to reduce electrostatic repulsion and the concentration was increased to 50×10^{-6} M to increase the supersaturation, repair still did not proceed (Figure S1, Supporting Information).

However, the height of the membranes then decreased by 48% from ≈ 4.8 to ≈ 2.5 nm, suggesting a major change in conformation.

Although single peptoid membranes on HOPG could not be repaired, repair was observed when a second membrane layer was present on top of the first layer (Figure 6). When the upper membrane was damaged, some gaps penetrated both layers down to the HOPG surface while others only penetrated the upper membrane, leaving the lower layer intact (Figure 6b). Nonetheless, upon exposure to 40×10^{-6} M pH

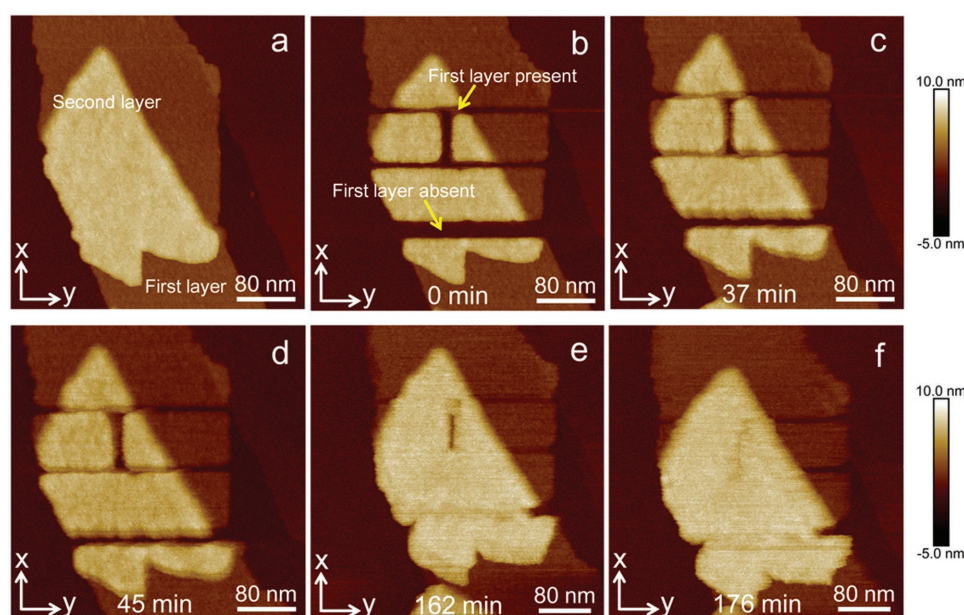


Figure 6. Self-repair of peptoid membranes on HOPG surfaces. a–f) In situ AFM images at different time points showing the anisotropic self-repair of the upper Pep-3 membrane in a stack of two Pep-3 membranes on HOPG with mechanically introduced defects along x -, y -directions. The region of damage indicated by lower arrow was intentionally enlarged relative to the other regions of damage to produce a longer period of repair and enable a more extensive investigation of the repair process in the absence of a lower layer.

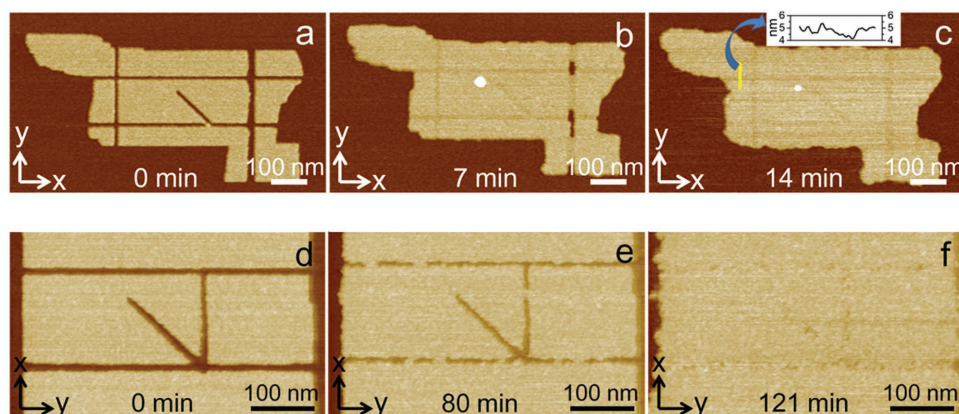


Figure 7. Membranes can be repaired using peptoid molecules with distinct hydrophilic domains and/or chain lengths. a–f) In situ AFM images at different time points showing repair of Pep-3 membranes on mica using: (a–c) Pep-2 solution and (d–f) Pep-4 solution.

2.6 Pep-3 monomer solution, the damage to the upper layer was repaired in both cases, even though no repair of the damaged regions in the lower layer was observed (Figure 6b–f). Following repair, the height of the newly formed region of the upper membrane was less than that of the undamaged region, suggesting that the gap in the lower membrane remained even after the upper membrane had been reconstituted (Figure 6c–f). As was the case for repair of Pep-3 membranes on mica or APS-mica in 10×10^{-6} M pH 4.3 Pep-3 solution, the upper layer repair proceeded in two stages, progressing slowly at first and then accelerating substantially (Figure 4b, Table 1).

Based on the structural model, the peptoid membranes investigated here are mainly stabilized by extensive π -stacking in the hydrophobic $N_{4-Cl}Pe$ region. In contrast, the hydrophilic headgroups are flexible and interact mainly through electrostatics.^[23] Consequently, repairing damaged membranes in solutions of monomers for which the functional group in the hydrophilic region is distinct from that of the original membrane may provide a route to forming multifunctional membranes. Moreover, by employing AFM-based nanoshaving^[29] to create the damage, the position of the new groups can be controlled with nm precision. To demonstrate this capability, peptoids Pep-2 and Pep-4, which have headgroup terminations that differ from that of Pep-3 (Figure 1a), were used for repair. The results show that both peptoids successfully assembled into the Pep-3 membranes and repaired the defects (Figure 7). In the case of Pep-2, because the length of the hydrophilic block is shorter than Pep-3, the resulting height of the repaired region was slightly lower than that of the original Pep-3 membrane (Figure 7c). In fact, repair of Pep-3 membranes by Pep-2 molecules occurred at a much higher rate than did Pep-3 self-repair under identical conditions (Table 1). Presumably the enhanced repair rate is a result of reduced steric repulsion due to the shorter chain length. In contrast, repair of Pep-3 membranes by Pep-4 molecules required a higher concentration and lower pH (Figure 4a, Table 1). These results show that the lipid-like design of these membranes enables the use of nanoshaving to create multifunctional membranes with nanoscale patterns of functional groups (Figure S2, Supporting Information).

3. Discussion

The results presented here highlight the significant impact that the mica surface has on the peptoid assembly process. Examination of the AFM images taken during the healing process shows that the outer edges of the membranes also advance (Figure 3c–f), but become considerably rougher than they are when they are initially deposited from the bulk solution. Indeed, other experiments show that the membranes grow from freshly made solutions of monomers directly onto mica substrates until the mica surface is completely covered, but that the growing 2D crystals have an approximately circular shape with a roughened edge.^[23] Taken together, these results show that, while the structure of the resulting membranes is determined by the peptoid–peptoid interactions, the kinetics of attaching and detaching at the growing edge are strongly impacted by the peptoid–mica interaction. The growth data imply that either the interaction is sufficiently stabilizing that it results in an isotropic edge free energy resulting in a rounded membrane, or it hinders the reversibility of binding so that the edge becomes kinetically roughened.

The results presented above have a number of implications for the role of peptoid protonation, surface charge, and substrate hydrophobicity in the repair process, the impact of hydrophobic surfaces on membrane structure, and the effect of the substrate more generally on the dynamics of peptoid self-assembly. At low pH (pH 2.6), the COOH groups are fully protonated, leading to favorable interactions such as hydrogen bonding among the COOH group side chains.^[30,31] These interactions can be expected to work in concert with the interactions within the hydrophobic block to synergistically contribute to the repair process and lead to relatively high repair rates (Figure 4a). At high pH (>4.3) the side chains become deprotonated to COO^- ,^[32] which should lead to inter-monomer electrostatic repulsion, acting against the repair process and reducing repair rates. In contrast, if the pH is maintained at 4.3 but the substrate is changed from bare mica to APS-treated mica, both of which are hydrophilic, there should then be an electrostatic attraction between the COO^- groups and the positively charged surface, leading to the observed increase in repair rate (Table 1).

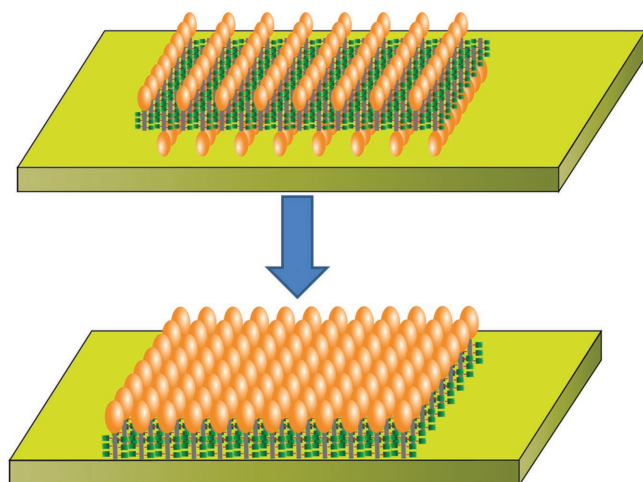


Figure 8. Schematic illustration of proposed change in membrane structure after deposition on HOPG, showing transformation from having the hydrophilic block pointing away from the substrate in *every other* row to having it point away in *every* row.

The introduction of HOPG, which is hydrophobic, alters both membrane structure and the ability of the membranes to self-repair. The observed 48% decrease in membrane thickness on HOPG upon exposure to low pH solution signals a structural change related to changes in peptoid-HOPG interactions. We hypothesize that, as in the case of assembly on mica, the protonated state of the hydrophilic blocks at low pH leads to favorable interactions such as hydrogen bonding among the COOH group side chains, while the hydrophobic nature of the substrate results in a favorable interaction between it and the peptoid hydrophobic blocks. As a result, the membrane structure should transform from having *every other* row oriented with the hydrophilic block pointing away from the substrate to having *every* row in this configuration (Figure 8). Because this structural change did not occur either on mica at low pH or on HOPG at high pH, we conclude that changes in both interactions are needed to affect the transformation. In contrast, because peptoid membranes in contact with HOPG (first layer) do not repair (Figure 6), even at low pH where repair on either bare or APS-treated mica does occur, we conclude that the interaction with the HOPG substrate is primarily responsible for inhibiting repair. This conclusion is reinforced by the observation that a second layer, which lacks contact with the HOPG surface, still exhibits self-repair.

Finally, we address the source of observed two-stage repair. The mechanism behind this process is revealed when the details of the membrane edges in the gap are examined more closely. The plots of repair rate vs. gap size are based on the average gap size. However, as Figure 5a–f shows, the membrane edges are not smooth during the repair process, but are rough. Consequently, even when there is still a finite average separation between the membrane edges, points of contact have already been established. The time at which the repair rate accelerates corresponds to the time at which these first points of contact occur. As Figure 5c,d illustrates, this creates regions of negative curvature, which then fill in rapidly in accordance with the Gibbs–Thomson effect, which relates states that the

chemical potential (and thus the supersaturation) scales exponentially with curvature.^[33] Due to the geometry of the damage, this negative curvature persists until the gap is completely eliminated. Hence the net repair rate remains large and constant throughout the 2nd stage of repair.

4. Conclusions

In summary, the findings reported here demonstrate that cell membrane-like 2D materials assembled from amphiphilic peptoids exhibit self-repair following mechanical damage. The rate of repair depends on a number of factors, including the charge state of the surface and peptoid headgroups, as well as the concentration of the solution used for repair. Depending on these factors, repair can occur in a single stage at constant rate, or in two stages in which the second stage proceeds as much as 160 times more rapidly due to the creation of negative curvature at points of contact between membrane edges. Hydrophilic substrates promote repair, while hydrophobic surfaces inhibit it and can, instead, cause the membrane to undergo a structural transformation. The ability of the upper membrane in a double-layer of membranes to exhibit self-repair on HOPG, even when the lower membrane has been removed during the damage process and cannot be repaired, suggests this AFM-based approach can provide information about the dynamics of molecular assembly in bulk solution—i.e., in the absence of a substrate. Finally, because membrane assembly is driven by the interactions between phenyl rings within the hydrophobic core,^[23] we can derive a general principle for design of self-repairing peptoid-based 2D materials: they should possess an identical sequence in the hydrophobic block, even if the hydrophilic block is distinct. As a result of this principle, nanoscale patterns of functional groups can be introduced into the membranes with nm-scale precision to produce multifunctional 2D materials by design and enable a wide range of applications.

5. Experimental Section

Peptoid Synthesis and Purification: Lipid-like peptoids were synthesized using a modified solid-phase submonomer synthesis method as described previously.^[34,35] They were either synthesized on a commercial Aapptec Apex 396 robotic synthesizer or manually synthesized in a 6.0 mL plastic vial. Peptoids were cleaved from the resin by addition of 95% trifluoroacetic acid (TFA) in water, and then dissolved in water and acetonitrile (v/v = 1:1) for HPLC purification (see Supporting Information in ref. [23] for details).

Self-Assembly of Peptoid Membranes: Lyophilized and HPLC-grade peptoids were dissolved in the mixture of water and acetonitrile (v/v = 1:1) to make 5.0×10^{-3} M clear solution, this clear solution was then transferred to 4 °C refrigerator for slow evaporation. Suspensions or gel-like materials containing a large amount of crystalline membranes were formed after a few days.

TEM Imaging: TEM samples were prepared by pipetting one drop of water diluted peptoid membrane gels or suspensions onto carbon-coated electron microscopy grid; 2% phosphotungstic acid was then used for negative staining. TEM was conducted on a 200-kV FEI Tecnai TEM microscope.

AFM Nanoshaving and Imaging: Preassembled Pep-3 membranes were first deposited on freshly cleaved mica, HOPG or freshly made APS-treated mica^[31] and incubated with water. Selected nanosheets

were purposely scribed using an AFM to create defects, and then freshly made peptoid solution with the pH adjusted by addition of HCl was injected into the fluid cell to initiate membrane repair. Both nanoshaving and image collecting were performed inside an enclosed fluid cell using silicon probes (HYDRA6V-100NG, $k = 0.292 \text{ N m}^{-1}$, AppNano) in ScanAsyst mode with a Nanoscope 8 (Bruker). During AFM imaging, to protect the sample, the force applied made as small as possible by adjusting the Peak Force Setpoint. The load force can be roughly calculated from the cantilever's spring constant, deflection sensitivity and Peak Force Setpoint.

Supporting Information

Supporting Information is available from the Wiley Online Library or from the author.

Acknowledgements

Peptoid synthesis was supported by the Materials Synthesis and Simulation Across Scales (MS³) Initiative through the LDRD program at Pacific Northwest National Laboratory (PNNL). In situ AFM studies were supported by the U.S. Department of Energy, Office of Basic Energy Sciences, Biomolecular Materials Program at PNNL. F.J. gratefully acknowledges financial support from China Scholarship Council. PNNL is multiprogram national laboratory operated for Department of Energy by Battelle under Contract No. DE-AC05-76RL01830.

Received: May 13, 2016

Revised: June 27, 2016

Published online: August 31, 2016

- [1] K. D. Zhang, J. Tian, D. Hanifi, Y. Zhang, A. C. Sue, T. Y. Zhou, L. Zhang, X. Zhao, Y. Liu, Z. T. Li, *J. Am. Chem. Soc.* **2013**, *135*, 17913.
- [2] K. Baek, G. Yun, Y. Kim, D. Kim, R. Hota, I. Hwang, D. Xu, Y. H. Ko, G. H. Gu, J. H. Suh, C. G. Park, B. J. Sung, K. Kim, *J. Am. Chem. Soc.* **2013**, *135*, 6523.
- [3] D. Moll, C. Huber, B. Schlegel, D. Pum, U. B. Sleytr, M. Sara, *Proc. Natl. Acad. Sci. USA* **2002**, *99*, 14646.
- [4] G. K. Olivier, A. Cho, B. Sanii, M. D. Connolly, H. Tran, R. N. Zuckermann, *ACS Nano* **2013**, *7*, 9276.
- [5] C. A. Palma, P. Samori, *Nat. Chem.* **2011**, *3*, 431.
- [6] G. R. Whittell, M. D. Hager, U. S. Schubert, I. Manners, *Nat. Mater.* **2011**, *10*, 176.
- [7] Z. Y. Tang, N. A. Kotov, S. Magonov, B. Ozturk, *Nat. Mater.* **2003**, *2*, 413.
- [8] J. Sakamoto, J. van Heijst, O. Lukin, A. D. Schluter, *Angew. Chem. Int. Ed.* **2009**, *48*, 1030.
- [9] J. W. Colson, W. R. Dichtel, *Nat. Chem.* **2013**, *5*, 453.
- [10] T. Bauer, Z. K. Zheng, A. Renn, R. Enning, A. Stemmer, J. Sakamoto, A. D. Schluter, *Angew. Chem. Int. Ed.* **2011**, *50*, 7879.
- [11] Y. J. Zheng, H. X. Zhou, D. A. Liu, G. Floudas, M. Wagner, K. Koynov, M. Mezger, H. J. Butt, T. Ikeda, *Angew. Chem. Int. Ed.* **2013**, *52*, 4845.
- [12] F. C. Zhang, F. Zhang, H. N. Su, H. Li, Y. Zhang, J. Hu, *ACS Nano* **2010**, *4*, 5791.
- [13] J. Sun, R. N. Zuckermann, *ACS Nano* **2013**, *7*, 4715.
- [14] R. J. Simon, R. S. Kania, R. N. Zuckermann, V. D. Huebner, D. A. Jewell, S. Banville, S. Ng, L. Wang, S. Rosenberg, C. K. Marlowe, D. C. Spellmeyer, R. Y. Tan, A. D. Frankel, D. V. Santi, F. E. Cohen, P. A. Bartlett, *Proc. Natl. Acad. Sci. USA* **1992**, *89*, 9367.
- [15] A. M. Rosales, H. K. Murnen, R. N. Zuckermann, R. A. Segalman, *Macromolecules* **2010**, *43*, 5627.
- [16] A. M. Rosales, R. A. Segalman, R. N. Zuckermann, *Soft Matter* **2013**, *9*, 8400.
- [17] K. Kirshenbaum, A. E. Barron, R. A. Goldsmith, P. Armand, E. K. Bradley, K. T. Truong, K. A. Dill, F. E. Cohen, R. N. Zuckermann, *Proc. Natl. Acad. Sci. USA* **1998**, *95*, 4303.
- [18] B. C. Lee, T. K. Chu, K. A. Dill, R. N. Zuckermann, *J. Am. Chem. Soc.* **2008**, *130*, 8847.
- [19] K. T. Nam, S. A. Shelby, P. H. Choi, A. B. Marciel, R. Chen, L. Tan, T. K. Chu, R. A. Mesch, B. C. Lee, M. D. Connolly, C. Kisielowski, R. N. Zuckermann, *Nat. Mater.* **2010**, *9*, 454.
- [20] R. Kudirka, H. Tran, B. Sanii, K. T. Nam, P. H. Choi, N. Venkateswaran, R. Chen, S. Whitelam, R. N. Zuckermann, *Biopolymers* **2011**, *96*, 586.
- [21] B. Sanii, R. Kudirka, A. Cho, N. Venkateswaran, G. K. Olivier, A. M. Olson, H. Tran, R. M. Harada, L. Tan, R. N. Zuckermann, *J. Am. Chem. Soc.* **2011**, *133*, 20808.
- [22] Z. Wu, M. Tan, X. Chen, Z. Yang, L. Wang, *Nanoscale* **2012**, *4*, 3644.
- [23] H. Jin, F. Jiao, M. D. Daily, Y. Chen, F. Yan, Y. Ding, X. Zhang, E. J. Robertson, M. D. Baer, C. Chen, *Nat. Commun.* **2016**, *7*, 12252.
- [24] Y. Duan, C. Wu, S. Chowdhury, M. C. Lee, G. M. Xiong, W. Zhang, R. Yang, P. Cieplak, R. Luo, T. Lee, J. Caldwell, J. M. Wang, P. Kollman, *J. Comput. Chem.* **2003**, *24*, 1999.
- [25] J. M. Wang, W. Wang, P. A. Kollman, D. A. Case, *J. Mol. Graph. Model.* **2006**, *25*, 247.
- [26] J. M. Wang, R. M. Wolf, J. W. Caldwell, P. A. Kollman, D. A. Case, *J. Comput. Chem.* **2004**, *25*, 1157.
- [27] S. Pronk, S. Pall, R. Schulz, P. Larsson, P. Bjelkmar, R. Apostolov, M. R. Shirts, J. C. Smith, P. M. Kasson, D. van der Spoel, B. Hess, E. Lindahl, *Bioinformatics* **2013**, *29*, 845.
- [28] Y. Roiter, S. Minko, *J. Phys. Chem. B* **2007**, *111*, 8597.
- [29] G. Y. Liu, S. Xu, Y. L. Qian, *Acc. Chem. Res.* **2000**, *33*, 457.
- [30] H. Cui, T. Muraoka, A. G. Cheetham, S. I. Stupp, *Nano Lett.* **2009**, *9*, 945.
- [31] P. Keim, R. A. Vigna, J. S. Morrow, R. C. Marshall, F. R. Gurd, *J. Biol. Chem.* **1973**, *248*, 7811.
- [32] Y. B. Sheng, W. Wang, P. Chen, *Protein Sci.* **2010**, *19*, 1639.
- [33] G. Cao, *Nanostructures and Nanomaterials: Synthesis, Properties and Applications*, Imperial College Press, London **2004**.
- [34] C.-L. Chen, J. Qi, J. Tao, R. N. Zuckermann, J. J. DeYoreo, *Sci. Rep.* **2014**, *4*, 6266.
- [35] R. N. Zuckermann, J. M. Kerr, S. B. H. Kent, W. H. Moos, *J. Am. Chem. Soc.* **1992**, *114*, 10646.